Simulation of the dynamical transmission of several-hundred-keV protons through a conical capillary

A. X. Yang, B. H. Zhu, S. T. Niu, P. Pan, C. Z. Han, H. Y. Song, J. X. Shao,[*] and X. M. Chen[†]

School of Nuclear Science and Technology, Lanzhou University, Lanzhou 730000, China

The time evolution of the trajectories, angular distributions, and two-dimensional images of intermediate-energy protons being transmitted through a conical capillary was simulated. The simulation results indicate that the charge deposited in the capillary significantly enhances the probability of surface specular scattering and thus greatly enhances the transmission rate. Furthermore, this deposited-charge-assisted specular reflection causes the transmission rate to exhibit an energy dependence proportional to E^{-1}, which is very consistent with the experimental data. After transmission at nonzero tilt angles, the angular distribution of several-hundred-keV protons is far from symmetric, unlike in the case of keV protons.

I. INTRODUCTION

Micro- and nanobeams are widely applied in physics, chemistry, biology, and materials science. Slow, highly charged ions can produce surface structures through the deposition of potential energy on the top surface layers of materials. Such beams have various applications, including nanoscale surface modification [1] and the shaping of ions beams [2]. Well-focused MeV/u beams with high potentials have been used for many purposes, such as in-air particle-induced x-ray emission analysis [3] and the irradiation of single living cells [4]. The energy loss and irradiation effects of several-hundred-keV/u ions interacting with materials are considerably stronger than those of keV and MeV ions. Such beams can be extensively applied in the controlled nanopatterning of material surfaces [5], microsurgery in living cells [6], and the controllable implantation of intermediate-energy protons in semiconductors [7,8].

The transmission of charged ions through a tapered or conical capillary can produce a high-density beam of microscopic dimensions. Ikeda [9] utilized the guiding effect of a single tapered capillary on charged particles [10] (highly charged ions and electrons) to produce a beam with a size of $\sim 2\,\mu$m. The density enhancement coefficient was as high as ~ 7 for an incident current of 0.2 pA without any electromagnetic lenses, and it decreased monotonically with increasing ion intensity. Zhou [11] studied the transmission features of 27 keV Ar^{9+} ions passing through a conical capillary and a tapered capillary and observed that the conical capillary provided stable transmission, whereas the tapered one did not. In 2003, Nebiki [12] performed an experiment investigating the transmission of 2 MeV He^+ ions through a tapered capillary and reported that small-angle scattering below the surface was dominant.

For intermediate energies of several hundred keV, in 2005, Vokhmyanina [13,14] experimentally explored the transmis-

sion process of $200-500$ keV protons through a conical capillary. It was found that the density enhancement coefficient F was ~ 5 at 200 keV, and decreased as $\sim E^{-1}$. The authors of [13,14] attempted to interpret the motion of these several-hundred-keV ions in terms of deposited charge from secondary electrons, but they did not succeed. Due to the lack of clear physical features, studies on the transmission of intermediate-energy ions through microcapillaries are of great value in both theory and application.

In this work, we present a simulation of $100-500$ keV protons being transmitted through a conical capillary. The simulated time evolution of the trajectories, angular distributions, and two-dimensional (2D) images of the transmitted particles is discussed. The transmission mechanism of a several-hundred-keV proton in the conical capillary is drawn from the simulation results. The simulation method is introduced in Sec. II, the simulation results are compared with experimental data and discussed in Sec. III, and the conclusions are presented in Sec. IV.

II. SIMULATION METHOD

Based on the experiment reported by Vokhmyanina [13], simulations were performed to study the transmission properties of $100-500$ keV protons in a conical capillary. Three types of forces should be considered [15] with regard to the transmission of intermediate-energy protons through a capillary. The first is the long-range Coulomb force from the surface charge deposited on the inner wall of the capillary. The second is the short-range collective scattering force from the topmost surface layer of atoms. The third is the binary encounter force between a projectile and target atoms below the inner surface of the capillary.

To ensure the accuracy of the calculations, the simulations were performed by solving the Hamilton equation using the Dormand-Prince numerical algorithm to obtain the ion trajectories. The ion trajectories in the conical (quartz) capillary were evaluated in three dimensions. The simulation parameters were obtained from previous experiments [13]. The entrance

diameter of the conical capillary was set to $d_{in} = 1.5$ mm and the exit diameter was set to $d_{out} = 0.5$ mm. The conical section was $L = 10$ cm long and had a cone angle of $0.28°$. The proton energies ranged from 100 to 500 keV, and the beam current I_{in} ranged from 0.1 to 2 μA [13] (the angular divergence of the incident beam was $\pm 0.1°$ half width at half maximum). Let the transmitted current be denoted by I_{out}; then, the density enhancement coefficient F can be expressed as

$$F = \frac{I_{out}/I_{in}}{(d_{out}/d_{in})^2}. \tag{1}$$

Before an incident proton penetrates into the inner surface of the capillary, the long-range Coulomb force H_{charge} from the surface charge patches and the short-range collective scattering force $H_{coll-scattering}$ from the surface layer of atoms simultaneously act on the proton. Therefore, the total Hamiltonian can be expressed as

$$H_{above} = H_{charge} + H_{coll-scattering}. \tag{2}$$

An incident proton within a critical distance of R_{exc} from the surface will capture an electron from the surface, thereby depositing a positive charge. The charge-exchange cross section between the 100 keV proton and an H_2O molecule is 1.2×10^{-16} cm^2 [16], and the cross section for an H_2 molecule is 2.1×10^{-17} cm^2 [17]. Then, the cross section for O is about 1.0×10^{-16} cm^2. According to the scaling law of a charge-exchange cross section [18,19] and Bragg's law, the averaged charge-exchange cross section between the 100 keV proton and the atoms in the SiO_2 molecule is 1.6×10^{-16} cm^2. Therefore, the charge-exchange distance of the 100 keV proton on the SiO_2 surface is estimated to be $R_{exc} \approx 1.35$ a.u. The polar angular distribution for secondary electrons emission from a surface follows a cosine law like in Refs. [20,21]. Most of the secondary electrons emit vertically from the surface. The positive charging due to impact ionization on one side of the capillary will be compensated by the low-energy secondary electrons from the opposite side of the capillary. Thus, the influence due to secondary electron emission was neglected.

The deposited charges are transported along the capillary via surface conductivity and into the bulk via bulk conductivity [22]. For a nanocapillary, both surface and bulk diffusion dominate the charge transport process; for a microcapillary, bulk conductivity dominates [23]. In our calculation, both bulk and surface conductivities were implemented and the bulk conductivity was described in detail. The time evolution of the deposited charge follows the equation

$$Q(r,t) = Q(r, t - \Delta t) \exp(-\Delta t/\tau_b), \tag{3}$$

where τ_b is the bulk discharge time constant and is expressed as

$$\tau_b^{-1} = \frac{2}{p(\varepsilon + 1)}. \tag{4}$$

Here, p is the specific resistivity and ε is the dielectric constant. For a normal glass capillary, the specific resistivity is $\sim 10^{11}$–10^{14} Ωm, and the dielectric constant is ~ 5–10. In the simulations of the guiding effect of glass reported by Schweigler [24] and Stolterfoht [25], the discharge times of the glass capillaries were ~ 2–5 min, and the calculated results were consistent with experimental data. In the present

study, the discharge time was taken to be 5 min. Notably, the transmission properties after equilibrium show almost no difference for discharge times between 2 and 5 min.

Because the direction of incidence was parallel to the axis of the capillary, the charge diffusion along the z dimension was simulated. The charge transport on the surface was implemented in the calculations as described in detail in a previous work [26] and references therein:

$$\Delta s = \Delta t \mu_0 E \exp\left(\sqrt{\frac{E}{E_c}}\right), \tag{5}$$

where Δt is the proton insertion time, μ_0 is the charge-carrier mobility, E is the electric field, and E_c is the characteristic field. For $E > E_c$, the transport length Δs exhibits an exponential (nonlinear) electric-field dependence, and for $E \ll E_c$, the electric-field dependence is linear (as in Ohm's law). The present simulations showed that the charge diffusion along the surface has little effect on the protons' transmission trajectories.

An average planar potential has previously been utilized to study the near-surface collective reflection of protons from graphite [27] and to describe a large fraction of transmitted neutrals [28]. Such a planar continuum potential is derived from a superposition of screened Coulomb potentials of the Thomas-Fermi type with the Molière screening function. In this paper, the scattering potential between a surface atom and an incident proton (hydrogen atom) is taken to be the Molière potential [27]:

$$V_{Moliere} = \frac{Z_p Z_t}{r}\{0.35 \exp(-0.3r/a) + 0.55 \exp(-1.2r/a)$$
$$+ 0.1 \exp(-6.0r/a)\}, \tag{6}$$

where $Z_p = 1$ is the charge of the incident particle, Z_t is the charge of the target atom (Si or O, in a SiO_2 capillary) [13], r is the distance from the incident particle to the target atom, and a is the screening parameter. In our calculations, the surface was defined as nonsmooth and the atoms in the surface layer were randomly arranged with an average atom spacing of d_0, where $d_0 = 4.6$ a.u. was obtained from the density and elemental composition of the target. In this random arrangement, the occurrence probabilities of Si and O atoms on the surface were determined by the chemical formula SiO_2 and were 33.3% and 66.7%, respectively.

When a proton penetrates the inner surface of the capillary, a series of stochastic binary encounters with single target atoms will occur. For simplicity and to reduce the calculation time, only elastic collisions with the Coulomb potential between two bare nuclei were used to calculate the scattering orbit. The differential scattering cross section is expressed by the Rutherford formula as follows:

$$\frac{d\sigma}{d\Omega} = \frac{(Z_p Z_t)^2}{E_m^2 16\sin^4(\theta/2)}. \tag{7}$$

After integration (with a minimum cutoff angle of θ_{min} [15]) of the differential scattering cross section, the total scattering cross section σ_t and the mean free path λ can be obtained. The Monte Carlo method was used to determine the positions and scattering directions of such a penetrating particle until the

particle emerged from the surface or was confirmed to remain in the bulk.

The incident beam current was $1\,\mu A/mm^2$, corresponding to the insertion of 1.1×10^{13} protons into the capillary every second. Considering the near-surface action, computing so many trajectories with high precision is a challenging task.

The following two approximations were used to improve computational efficiency. (1) The reduced-size approximation: the size of the capillary used in the calculation was reduced in equal proportion to the original size of the conical macrocapillary ($d_{in} = 1.5\,mm$, $d_{out} = 0.5\,mm$, $L = 10\,cm$). The size of the capillary was varied using one-tenth, one-hundredth, and one-thousandth of the original size. (2) The accelerated charge-up approximation: tens to one-thousand ion charges were

assumed to be deposited per ion hitting as in previous research of keV ion transmission in a conical macrocapillary [25]. From test calculations, we can reach the conclusion that these two approximations do not influence the calculation accuracy and can extremely improve the computational efficiency.

For good accuracy and also high efficiency, most of the present results were obtained with the parameters ($d_{in} = 1.5\,\mu m$, $d_{out} = 0.5\,\mu m$, $L = 100\,\mu m$) of one-thousandth of the original size and without charge-up acceleration. Proton insertion was treated sequentially in small portions (typically $\Delta n = 1100$). After $\Delta n = 1100$ ions were inserted into the capillary, the deposited charges were attenuated during the insertion time of the Δn ions. The number of deposited charges was defined as $q_d = mq$ ($m = 1$). Thus, the insertion
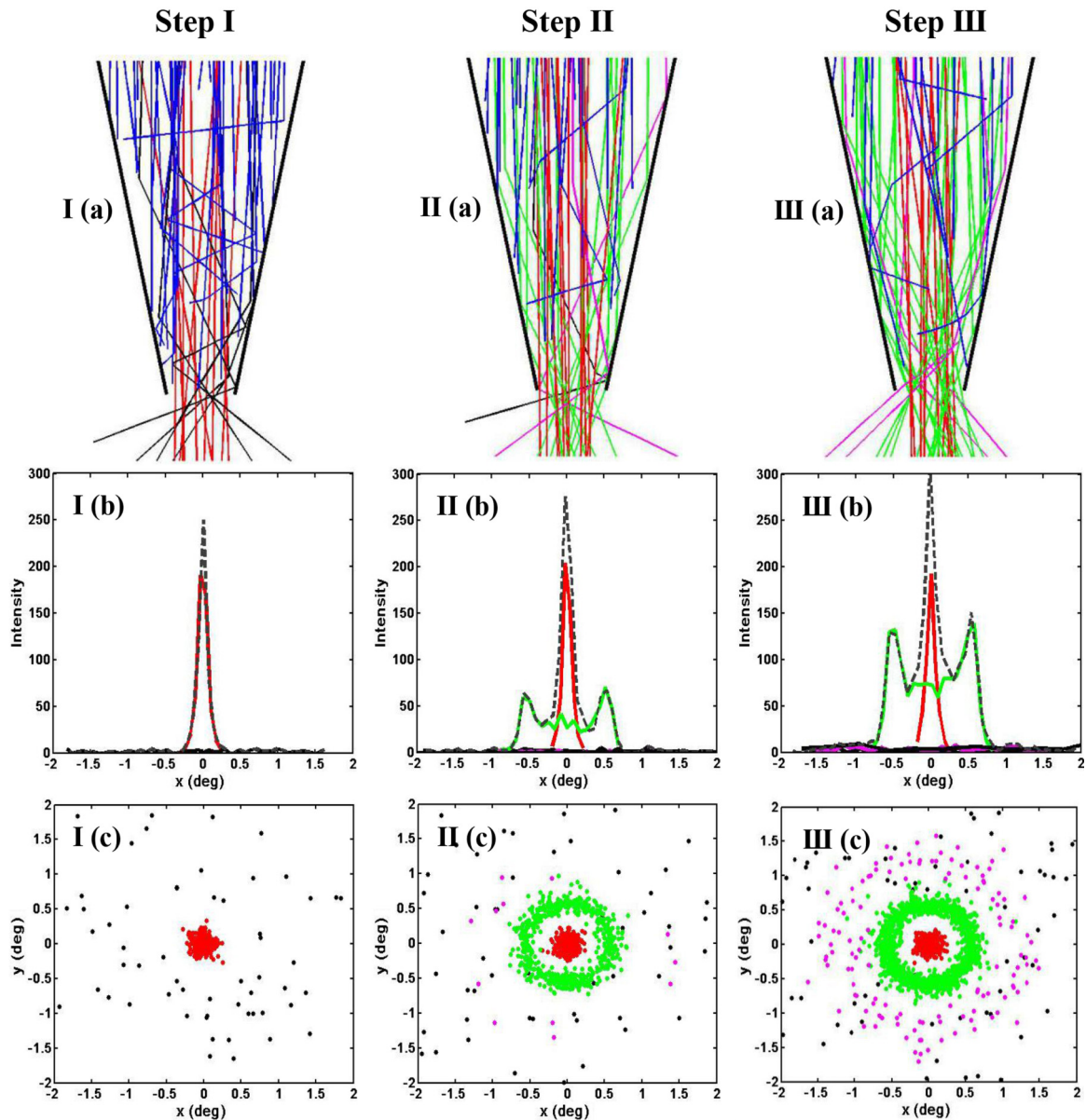
FIG. 1. The simulated trajectories, angular distributions, and 2D images of 100 keV protons passing through a conical capillary with a tilt angle of $0°$: at the beginning (step I), during the charge-up process (step II), and after equilibrium (step III). The red, green, magenta, and black lines and dots represent direct transmission, single surface specular reflection, double surface specular reflection, and multiple scattering at and below the surface, respectively. The blue lines represent proton trajectories that stopped inside the capillary wall. The parameters of each conical capillary in the upper part were $d_{in} = 1.5\,\mu m$, $d_{out} = 0.5\,\mu m$, and $L = 100\,\mu m$.

time is given by

$$\Delta t = \frac{q_d \Delta n}{I_{\text{in}}}. \tag{8}$$

As noted, the incident beam current was $I_{\text{in}} = 1\,\mu\text{A/mm}^2$, corresponding to $\Delta t = 0.0001\,\text{s}$ with $\Delta n = 1100$.

III. RESULTS AND DISCUSSION

The time evolution of the trajectories, angular distributions, and 2D images of 100 keV protons being transmitted through a conical capillary with a tilt angle of 0° was calculated, and the results are presented in Fig. 1. The calculations were performed as described in Sec. II. Each panel in the upper half of the figure illustrates 50 typical trajectories.

Initially [see panel I(c) of Fig. 1], the 2D image consists of two components: a red core at the center and some scattered black dots far from the center. From the projection of this 2D image onto the x axis, as shown in panel I(b) of Fig. 1, we can see that the red core is a high Gaussian peak superimposed on a low and broad baseline. As shown in panel I(a) of Fig. 1, the red core is formed by directly transmitted particles, whereas the black dots represent the particles that are transmitted through the capillary via multiple scattering at or below the surface. The height of the black baseline is approximately two orders of magnitude lower than that of the red Gaussian peak. This distribution is similar to that of high-energy ions transmitted through a tapered glass capillary [12].

After some charge has been deposited on the inner surface of the capillary, the 2D image of the transmitted particles in Fig. 1, panel II(c), is obviously different from the initial distribution. A green circle appears near the angles of $\pm 0.56°$, and some magenta dots are seen around the green circle. From the projection of the 2D image onto the x axis in Fig. 1, panel II(b), we can see that the green circle forms two distinct peaks on the left and right sides of the directly transmitted beam. As seen from the green trajectories in Fig. 1, panel II(a), the green circle is formed by particles that are transmitted through the capillary via a single specular reflection at the surface. Thus, the two peaks appear at positions of $\pm 0.56°$, twice the cone angle of the capillary. The small number of magenta dots corresponds to particles transmitted via two specular reflections. The height of the two green peaks is equal to one-third of that of the central red Gaussian peak. These peaks form because the deposited charge enhances the probability of surface specular scattering and causes more protons' trajectories to look like "mirror reflections."

As in Fig. 1, step III, the number of inserted protons amounts to $\sim 1.2 \times 10^5$ for which equilibrium was achieved. The 2D image of the transmitted particles has four main components. In addition to the scattered black dots, a magenta circle appears near angles of $\pm 1.2°$. This indicates that under the continuous assistance of the deposited charge, trajectories with two specular reflections at the surface start to play a more significant, though still minor, role. As shown in Fig. 1, panel III(a), with the further assistance of the deposited charge, the majority of the transmitted particles passes through the capillary via a single surface specular reflection. As a result, as seen from Fig. 1, panel III(b), the two green peaks at $\pm 0.56°$ become the most important, with a significant increase in
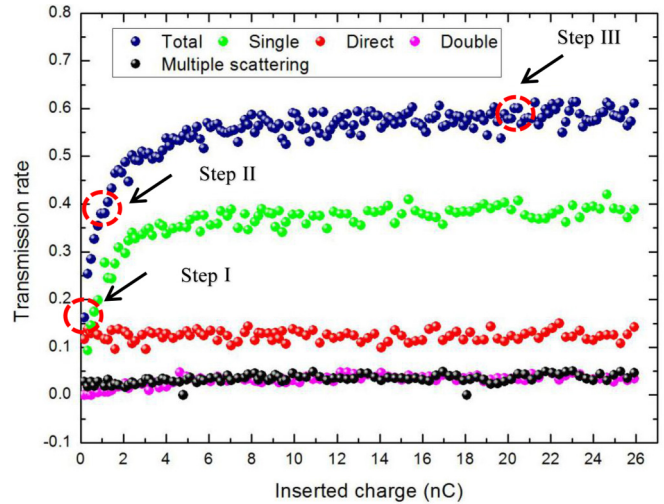
FIG. 2. Calculated time evolution of the total transmission rate (blue dots), the direct transmission rate (red dots), the transmission rate for single specular reflection (green dots), the transmission rate for double specular reflection (magenta dots), and the transmission rate for multiple scattering at and below the surface (black dots) of 100 keV protons at a tilt angle of 0°. The horizontal axis represents the inserted charge in the original macrocapillary, which is derived from the charge in the reduced-size capillary.

height compared with step II. The two green peaks are one order of magnitude higher than the magenta line. The intensity of the central red Gaussian peak remains stable throughout the entire charging-up process. These findings indicate that the guiding effect disappears for 100 keV protons, which is consistent with the results of a previous 200 keV H_2^+ transmission experiment [29].

The calculated transmission rates of 100 keV protons for different processes are plotted in Fig. 2, including those for single and double charge-patch-assisted specular reflection and multiple scattering at or below the surface as well as the total transmission rate. The transmission rates are obtained as the numbers of transmitted protons via different processes normalized to the number of incident protons. Initially, the total transmission rate is approximately 0.15, and approximately 80% of the transmitted particles pass through the capillary directly, whereas the remaining 20% undergo multiple scattering at or below the surface of the capillary. Almost no particles pass through the capillary via single or double specular reflection. As the inserted charge increases to approximately 1 nC, the total transmission rate rises from the initial value of 0.15 to 0.4. Approximately 57% of the transmitted particles undergo single charge-patch-assisted specular reflection, and 4% of them undergo double specular reflection, whereas 32% of them are directly transmitted. The contribution of multiple scattering is always small and less than 7%. As the inserted charge increases to several tens of nC, transmission equilibrium is achieved. Under these conditions, the total transmission rate reaches 0.6, which is $\sim 5-6$ times larger than the direct transmitted value. Approximately 65% of the transmitted particles pass through the capillary via a single specular reflection at the surface. These findings indicate that with the assistance of the deposited charge, the process of single specular reflection controlled
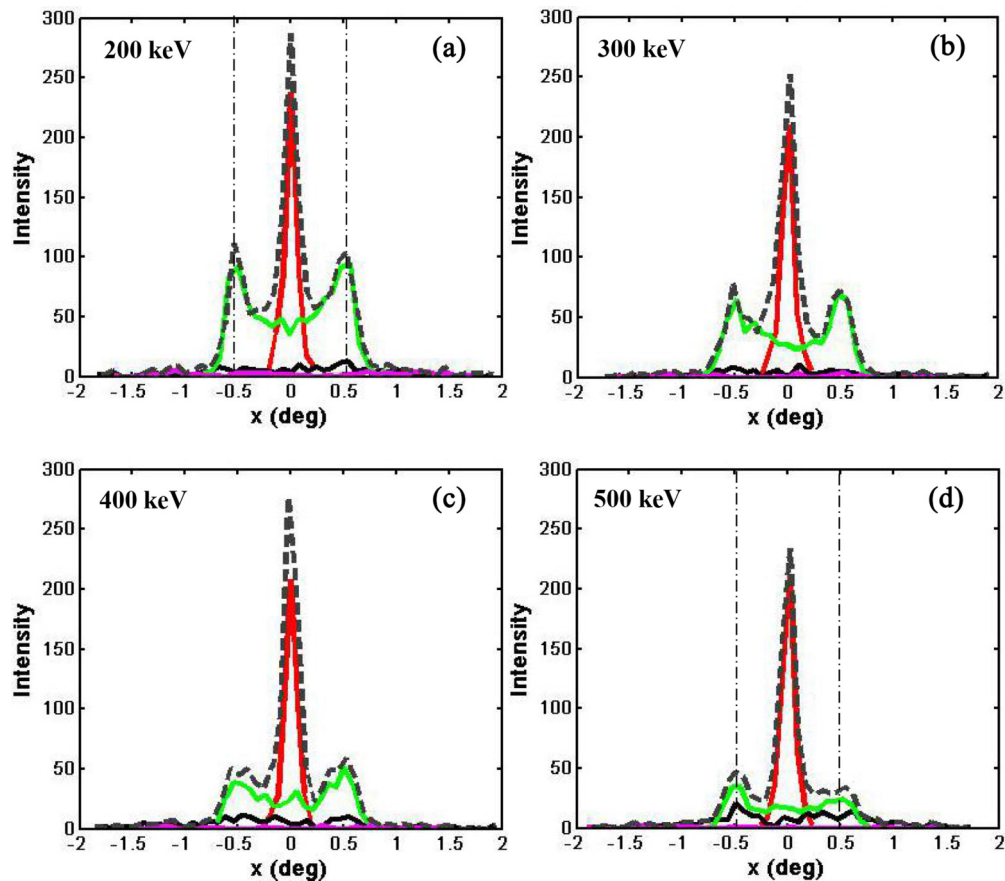
FIG. 3. Simulated angular distributions of the transmitted particles after equilibrium when 200−500 keV protons are passing through a conical capillary with a tilt angle of 0°.

by the collective scattering forces near the surface comes to dominate the transmission of 100 keV protons through a conical capillary. By contrast, direct transmission, double specular reflection, and multiple scattering are of less importance; they contribute only 21%, 7%, and 7%, respectively, to the total transmission after equilibrium.

To illustrate the energy dependence of the transmission properties for several-hundred-keV protons, the calculated angular distributions and transmission rates after equilibrium are presented in Figs. 3 and 4, respectively. From Figs. 3(a)–3(d), it is seen that the angular distributions of transmitted protons at these energies all consist of two main components, namely, a red peak at the center and two side peaks near ±0.56°, similar to the 100 keV case. The intensity of the two side peaks gradually decreases as the incident energy increases. In addition, the centroid positions of the two side peaks shift just slightly closer to zero degrees as the incident energy increases from 100 to 500 keV.

From Fig. 4, we can observe the contributions of the different processes to the total transmission rate after equilibrium. For 200 keV protons, the total transmission rate decreases from 0.6 in the 100 keV case to the value of 0.49, and approximately 56% of transmitted particles pass through the capillary via single specular reflection. When the energy increases to 300 keV, the total transmission rate decreases to 0.37 and, correspondingly, 50% of the transmitted particles are transmitted via single specular reflection. For an incident

energy of 500 keV, the total transmission rate is only 0.27, and the contribution from single specular reflection is only 34% of the total, which is smaller than the contribution from direct transmission. Throughout this entire energy region, the
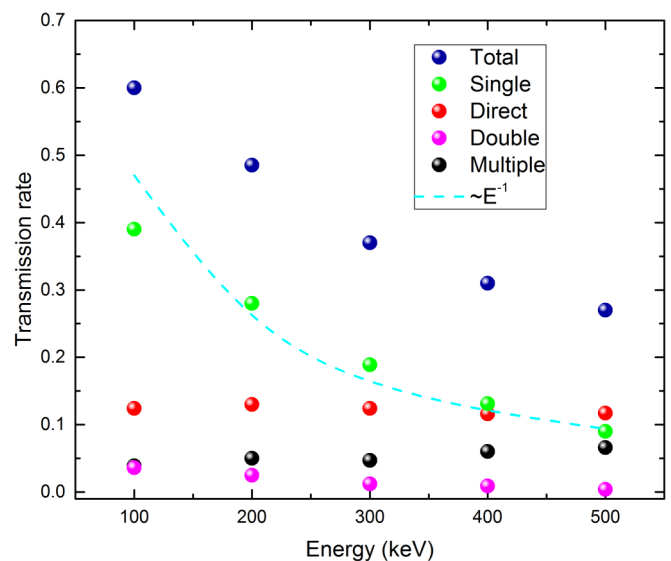
FIG. 4. Calculated energy dependence of the total transmission rate and its four components after equilibrium when 100−500 keV protons are passing through a conical capillary with a tilt angle of 0°.

TABLE I. Comparison of the values of the density enhancement coefficient F from these simulations and from experimental data [13] for different incident proton energies.

Energy (keV)	100	200	300	400	500
This work (enhancement coefficient F)	5.45	4.45	3.36	2.91	2.45
Experiments [13]		4.90	3.27	2.90	2.0

contributions from double specular reflection and multiple scattering are much smaller, corresponding to less than 25% of the total transmission rate.

In Fig. 4, the transmission rate corresponding to single specular reflection exhibits a dependence of E^{-1}. Hence, the energy dependence of the total transmission rate is also expected to be approximately proportional to E^{-1}, which is consistent with previous experimental data for the transmission of $200-500$ keV protons through a conical capillary [13].

The calculated values of the density enhancement coefficient F for different proton energies at a tilt angle of $0°$ are presented in Table I and compared with the experimental data from Ref. [13]. The simulations are in excellent agreement with the experiments. The enhancement coefficients F in the several-hundred-keV region are larger than those for energies of several MeV [30,31]. For several-hundred-keV ions, the deposited charge enhances surface specular reflection and thus significantly enhances the transmission rate. By contrast, for MeV ions, only multiple scattering due to binary encounters below the surface [30,31] can provide some limited enhancement of the transmission rate.

To obtain more information on the transmission of several-hundred-keV protons through conical capillaries with different tilt angles, the angular distributions and 2D images of the transmitted particles after equilibrium were calculated for 100 keV protons at tilt angles of $0°$, $0.2°$, and $0.4°$, and the results are presented in Fig. 5. The results for the 10 keV proton case were also calculated and are presented in Fig. 6 to illustrate the differences.

In Fig. 5(a), for a tilt angle of $0°$, the pair of green peaks at $\pm 0.56°$ lies symmetrically on the left and right sides of the directly transmitted beam. When the tilt angle is increased to $0.2°$, the distribution of the two green peaks becomes extremely asymmetric. The left-hand peak moves to $-0.25°$ and is much higher than the right-hand peak at $0.85°$. In Fig. 5(c), for a tilt angle of $0.4°$, the two green peaks become much flatter and broader, resulting in two small peaks lying at $0°$ and $1.4°$.

From Figs. 5(d)–5(f), we can see that as the tilt angle increases, the position of the directly transmitted beam does not change. However, the green circle, corresponding to single charge-patch-assisted specular reflection, moves with the tilt direction and broadens along the x axis. As the tilt angle increases, the left half of the magenta circle originating from double surface specular reflection gradually disappears, while the right half remains. This behavior is probably due to the geometric limitations of the capillary at large tilt angles. The simulation results indicate that the value of the density enhancement coefficient F rapidly decreases as the tilt angle increases. The values of F are 5.45 at $0°$, 4.36 at $0.2°$, and 2.18 at $0.4°$. From a comparison between Figs. 5 and 6, it is obvious that the transmission properties of 100 keV protons at various
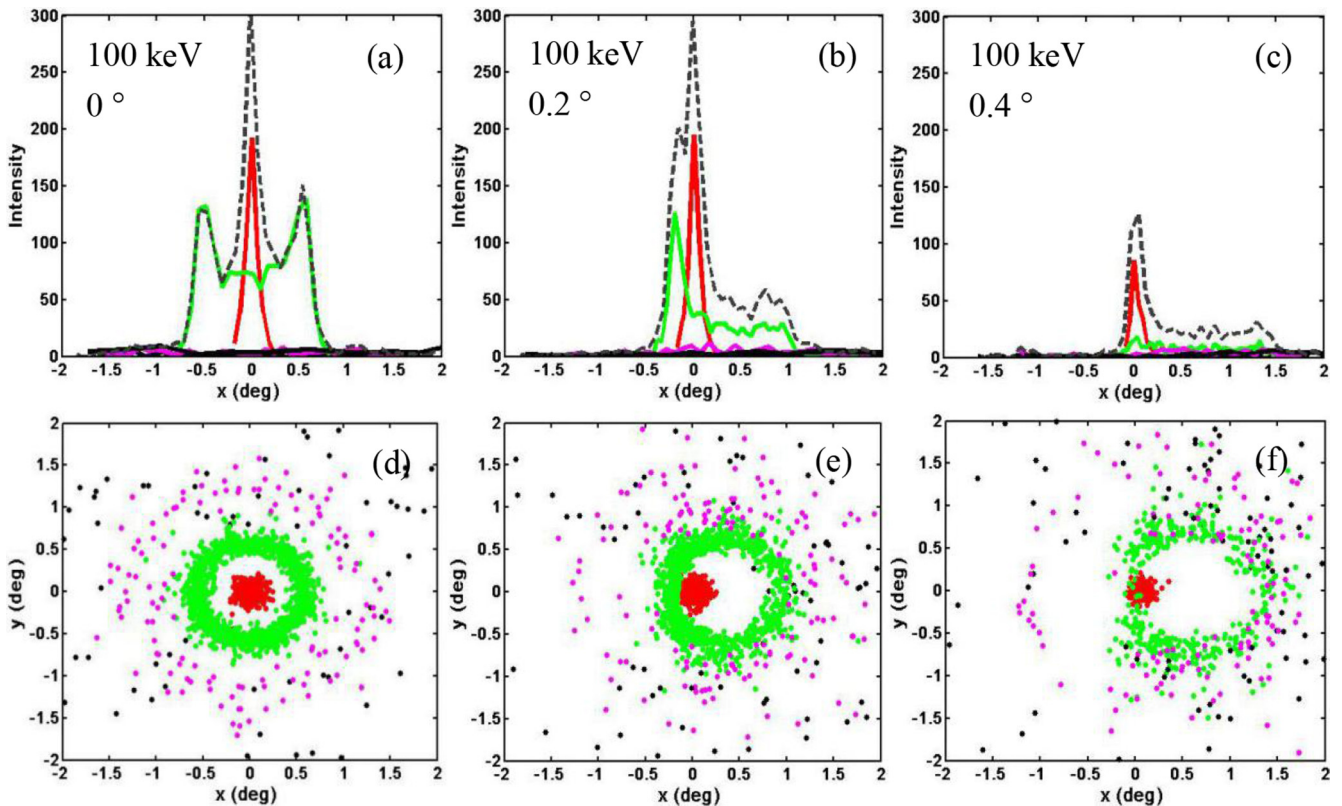
FIG. 5. Simulated angular distributions and 2D images of the transmitted particles after equilibrium when 100 keV protons are transmitted through conical capillaries with tilt angles of $0°$, $0.2°$, and $0.4°$.
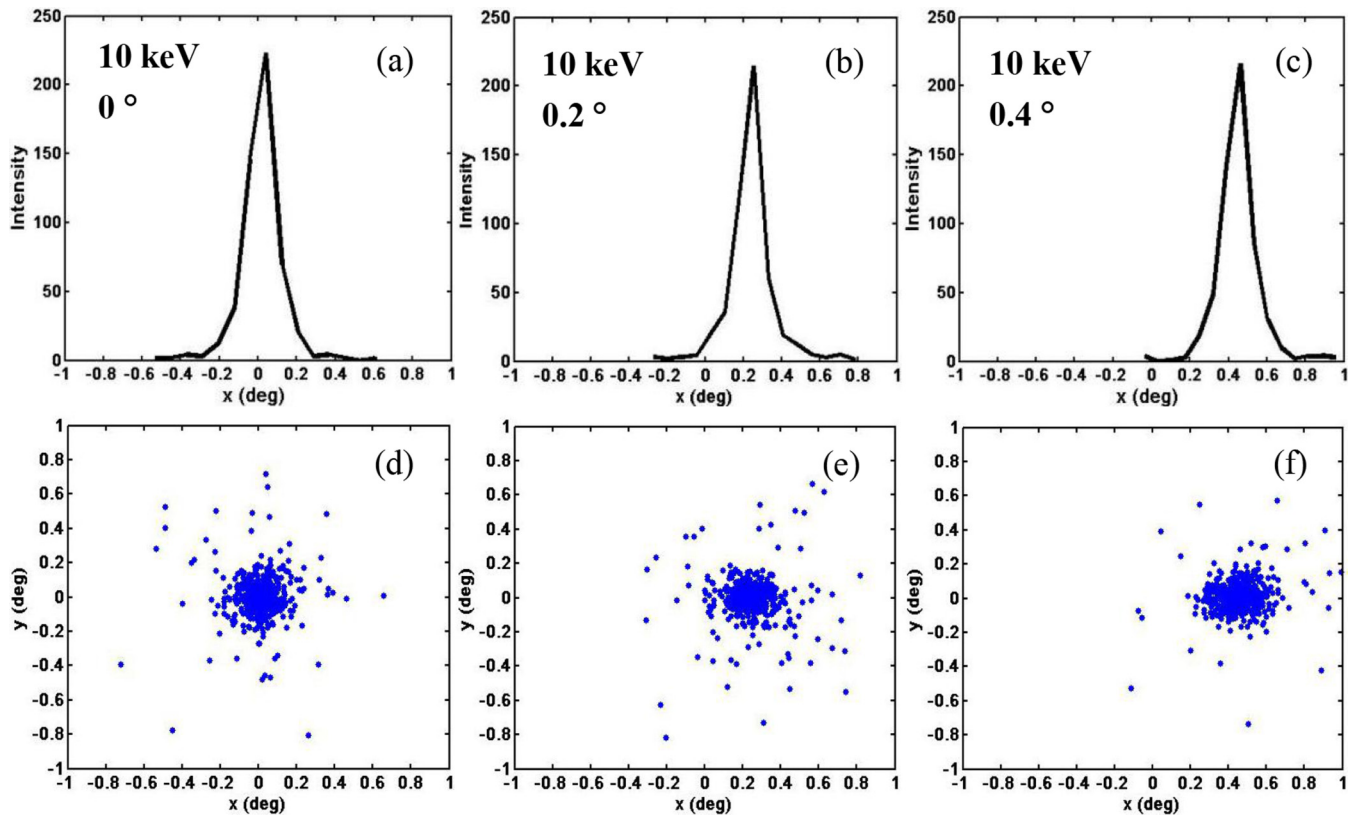
FIG. 6. Simulated angular distributions and 2D images of the transmitted particles after equilibrium when 10 keV protons are transmitted through conical capillaries with tilt angles of 0°, 0.2°, and 0.4°.

tilt angles are completely distinct from those of 10 keV protons. Figure 6 shows that 10 keV protons can be effectively guided by a tilted capillary and that the distribution of the transmitted particles has a single-peak structure. The peak intensity does not change much as the tilt angle is increased from 0° to 0.4°.

IV. CONCLUSION

In this work, the transmission through a conical capillary of protons with energies of $100-500$ keV was simulated. The simulation results are in excellent agreement with the available experimental data. Ions with energies of several hundreds of keV can be transmitted through a capillary via four different processes: (1) direct transmission, (2) single surface specular reflection, (3) double surface specular reflection, and (4) multiple scattering at or below the inner surface of the capillary. During the charging-up process, the charge deposited in the capillary will significantly enhance the probability of single surface specular reflection and thus greatly enhance the transmission rate. For this reason, the density enhancement coefficient F for $100-200$ keV protons can be as high as $\sim 5-6$, and the coefficient F also shows an energy dependence proportional to E^{-1}. When the conical capillary is tilted, the transmission properties of several-hundred-keV ions are completely different from those of keV ions. The latter can be effectively guided by a tilted capillary, whereas the former cannot. For several-hundred-keV ions, as the tilt angle increases, the position of the directly transmitted beam does not change; however, the distribution of the particles that are transmitted via charge-patch-assisted surface specular reflection broadens and shifts along the tilt direction.

[1] L. P. Ratliff, R. Minniti, A. Bard, E. W. Bell, J. D. Gillaspy, D. Parks, A. J. Black, and G. M. Whitesides, Appl. Phys. Lett. **75**, 590 (1999).

[2] H.-Q. Zhang, N. Akram, P. Skog, I. L. Soroka, C. Trautmann, and R. Schuch, Phys. Rev. Lett. **108**, 193202 (2012).

[3] N. Fujita, K. Ishii, and H. Ogawa, Nucl. Instrum. Methods Phys. Res. B **269**, 1023 (2011).

[4] V. Maeckel, W. Meissl, T. Ikeda, M. Clever, E. Meissl, T. Kobayashi, T. M. Kojima, N. Imamoto, K. Ogiwara, and Y. Yamazak, Rev. Sci. Instrum. **85**, 014302 (2014).

[5] C. T. Nguyen, A. Balocchi, D. Lagarde, T. T. Zhang, H. Carrere, S. Mazzucato, P. Barate, E. Galopin, J. Gierak, E. Bourhis, J. C. Harmand, T. Amand, and X. Marie, Appl. Phys. Lett. **103**, 052403 (2013).

[6] Y. Iwai, T. Ikeda, T. M. Kojima, and Y. Yamazaki, Appl. Phys. Lett. **92**, 023509 (2008).

[7] S. J. Pearton, J. W. Corbett, and M. Stavola, *Hydrogen in Crystalline Semiconductors* (Springer-Verlag, Berlin, 1992).

[8] Xiao Qing-hua, Wang Jing, and Tu Hai-ling, *Proceedings of the Fifth Annual Academic Meeting of China Nonferrous Metals Society*, doi:10.13827/j.cnki.kyyk.2003.s1.062.

[9] T. Ikeda, Y. Kanai, T. M. Kojima, Y. Iwai, T. Kambara, and Y. Yamazaki, Appl. Phys. Lett. **89**, 163502 (2006).

[10] N. Stolterfoht, J. H. Bremer, V. Hoffmann, R. Hellhammer, D. Fink, A. Petrov, and B. Sulik, Phys. Rev. Lett. **88**, 133201 (2002).

[11] C. L. Zhou, M. Simon, T. Ikeda, S. Guillous, W. Iskandar, A. Mery, J. Rangama, H. Lebius, A. Benyagoub, C. Grygiel, A. Muller, M. Dobeli, J. A. Tanis, and A. Cassimi, Phys. Rev. A **88**, 050901(R) (2013).

[12] T. Nebiki, T. Yamamoto, T. Narusawa, M. B. H. Breese, E. J. Teo, and F. Watt, J. Vac. Sci. Tech. A: Vacuum Surf. Films **21**, 1671 (2003).

[13] K. A. Vokhmyanina, L. A. Zhilyakov, A. V. Kostanovsky, V. S. Kulikauskas, V. P. Petukhov, and G. P. Pokhil, J. Phys. A: Math. Gen. **39**, 4775 (2006).

[14] K. A. Vokhmyanina, L. A. Zhilyakov, A. V. Kostanovsky, V. S. Kulikauskas, V. P. Petukhov and G. P. Pokhil, Proc. SPIE **5943**, 594304 (2005).

[15] G. Y. Wang, J. X. Shao, Q. Song, D. Mo, A. X. Yang, X. Ma, W. Zhou, Y. Cui, Y. Li, Z. L. Liu, and X. M. Chen, Sci. Rep. **5**, 15169 (2015).

[16] L. F. Errea, Clara Illescas, L. Méndez, B. Pons, I. Rabadán, and A. Riera, Phys. Rev. A **76**, 040701(R) (2007).

[17] Clara Illescas and A. Riera, Phys. Rev. A **60**, 4546 (1999).

[18] M. E. Rudd, R. D. DuBois, L. H. Toburen, C. A. Ratcliffe, and T. V. Goffe, Phys. Rev. A **28**, 3244 (1983).

[19] W. R. Thompson, M. B. Shah, and H. B. Gilbody, J. Phys. B: At. Mol. Opt. Phys. **29**, 725 (1996).

[20] D. Hasselkamp, H. Rothard, K.-O. Groeneveld, J. Kemmler, P. Varga, and H. Winter, Springer Tracts Mod. Phys. **123**, 1 (1991).

[21] J. Mischler, N. Benazeth, M. Negre, and C. Benazeth, Surf. Sci. **136**, 532 (1984).

[22] K. Schiessl, W. Palfinger, K. Tokesi, H. Nowotny, C. Lemell, and J. Burgdorfer, Phys. Rev. A **72**, 062902 (2005).

[23] N. Stolterfoht, Phys. Rev. A **89**, 062706 (2014).

[24] T. Schweigler, C. Lemell, and J. Burgdorfer, Nucl. Instrum. Methods Phys. Res. B **269**, 1253 (2011).

[25] N. Stolterfoht, E. Gruber, P. Allinger, S. Wampl, Y. Wang, M. J. Simon, and F. Aumayr, Phys. Rev. A **91**, 032705 (2015).

[26] N. Stolterfoht, Phys. Rev. A **87**, 012902 (2013).

[27] R. Pfandzelter and F. Stolzle, Nucl. Instrum. Methods Phys. Res. B **72**, 163 (1992).

[28] H. Q. Zhang, N. Akram, and R. Schuch, Phys. Rev. A **94**, 032704 (2016).

[29] S. D. Liu, Y. Y. Wang, Y. T. Zhao, X. M. Zhou, R. Cheng, Y. Lei, Y. B. Sun, J. R. Ren, J. L. Duan, J. Liu, H. S. Xu, and G. Q. Xiao, Phys. Rev. A **91**, 012714 (2015).

[30] J. Hasegawa, S. Jaiyen, C. Polee, N. Chankow, and Y. Oguri, J. Appl. Phys. **110**, 044913 (2011).

[31] F. Hespeels, R. Tonneau, T. Ikeda, and S. Lucas, Nucl. Instrum. Methods Phys. Res. B **362**, 72 (2015).